Available online at www.sciencedirect.com

SCIENCE DIRECT

Biochimica et Biophysica Acta 1716 (2005) 1 – 10

BIOCHIMICA ET BIOPHYSICA ACTA
BBA

http://www.elsevier.com/locate/bba

Computational analysis of mutations in the transmembrane region of Vpu from HIV-1

Andrew Candler, Matthew Featherstone, Rehan Ali, Leslie Maloney, Anthony Watts, Wolfgang B. Fischer*,[1]

Biomembrane Structure Unit, Department of Biochemistry, Oxford University, South Parks Road, Oxford OX1 3QU, UK

Received 16 February 2005; received in revised form 27 June 2005; accepted 28 July 2005
Available online 16 August 2005

Abstract

Vpu is an 81 amino acid integral membrane protein encoded by HIV-1. Its α-helical transmembrane (TM) domain (residues ~6–28) enhances virion release by oligomerizing into bundles and forming ion-conducting channels across the plasma membrane. Its cytoplasmic domain (residues ~29–81) is also α-helical and binds to the transmembrane protein CD4, inducing its degradation. Mutations within the TM domain have been found to abrogate enhanced particle release from the infected cell (Tiganos et al. *Virology* (1998) 251 96–107). A series of computational models of monomeric, pentameric and hexameric Vpu_{1-31} mutants have been constructed, embedded in fully hydrated lipid bilayers and subjected to a 3 ns molecular dynamics (MD) simulation. None of the mutations has any destabilizing effect on the secondary and tertiary structure. One of the mutants, in which the position of a tryptophan residue within the TM domain is altered, is known not to induce CD4 degradation; an extended kinked model of this mutant has been generated (Vpu_{1-52}IVW-k) and during subsequent MD simulations, the bend between the TM and a part of the cytoplasmic domain is found to unwind and a complex salt bridge involving Lys-37 is formed.

Keywords: Vpu; HIV-1; Mutant; Viral membrane protein; Molecular dynamics simulation; protein structure

1. Introduction

Computational methods such as molecular dynamics (MD) simulations can be used to assess whether any mutation in a protein has an effect on the structure and function of the protein before more time consuming experiments have been performed. Recently, MD simulations have been used to perform a computational alanine scanning experiment on the 1:1 human growth hormone–receptor complex [1]. It was shown that the simulation results are in good agreement with the experimental findings of binding free energy differences. In another study, the structural impact of mutations in the fusion domain of the fusion protein gp41 from HIV-1 on its fusogenic activity has been explored [2]. As a result of the simulations, conformational flexibility was suggested as the key factor which might be responsible for the experimental findings [3]. Here, mutants of the viral membrane protein Vpu from HIV-1 are used to evaluate possible implications of these mutations on the structural integrity.

Vpu is a type I integral membrane protein of 81 amino acids with a N terminal transmembrane (TM) domain and a larger cytoplasmic domain ([4–6], reviewed in [7]). The protein acts in two ways: (i) by interaction of its cytoplasmic domain with CD4 which leads to a degradation of CD4 [8–11], (ii) by self-assembly which induces ion channel activity to amplify the release of immature virions from the infected cell [12,13]. The structure of Vpu is reasonably well resolved by NMR [14–17], CD- [18] and FTIR-spectroscopy [19], enabling the generation of working

* Corresponding author. Tel.: +44 1865 275776; fax: +44 1865 275234.
E-mail address: wolfgang.fischer@bioch.ox.ac.uk (W.B. Fischer).
[1] Current address: Bionanotechnology IRC, Clarendon Laboratory, Department of Physics, Oxford, University, Oxford, OX1 3PU, UK.

0005-2736/$ - see front matter © 2005 Elsevier B.V. All rights reserved.
doi:10.1016/j.bbamem.2005.07.012

a model for Vpu which can be summarized as follows: a TM helix approximately from residue 6 to 29, a second helix (helix-2) from residue 40 to 50 and a third helix (helix-3) from residue 60 to 70. Another short helix or turn is proposed for residues 75 to 78. Using this information, models can be produced for computational analysis.

In this study, experimental investigations on TM domain mutants of Vpu and the consequences of these mutations on its structure are explored using MD simulations. Mutations within the TM domain have been found to modulate the ability of Vpu to enhance particle release [20]. The present exploration serves as a test case to assess the mechanism of this function on an atomic scale. For all of the mutants investigated, membrane integration ability and subcellular translocation was identical to wild type (WT) Vpu [20]. In addition to a modulation of particle release, one mutant also abrogates CD4 degradation. The structural integrity of the TM helix has been found to be essential for both functions of Vpu [20]. Generation of computational models with solely the TM domain (TM helix), either as a single entity or as a pentameric or hexameric assembly embedded in a hydrated lipid bilayer, aims to assess whether these mutations would affect local conformation of the TM domain of the protein. An extended model of Vpu including the first 52 amino acids of one of the mutants is generated because of the dual effect of this mutant: reducing particle release and failing to induce CD4 degradation [20]. The simulation time is held short to enable a large number of models to be produced on a computationally low-cost level.

2. Materials and methods

Wild type Vpu_{1-31} (HV1H2) and a series of mutant single helices consisting of the first 31 residues of Vpu (for simplicity referred to as WT-1, FV-1, respectively) and bundles consisting of five (WT-5, FV-5) and six of these helices (WT-6, FV-6) were generated. For one mutant, Vpu-IVW, an extended model with 52 amino acids, referred to as IVW-k, was generated.

The sequences used for the models are:

WT	QPIQIAIVA^{10} LVVAIIIAIV^{20} VWSIVIIEYR^{30} K
FI mutant	QPIQIA**FI**A^{10} LVVAIIIAIV^{20} VWSIVIIEYR^{30} K
KSL mutant	QPIQ**K**A**SL**A^{10} LVVAIIIAIV^{20} VWSIVIIEYR^{30} K
FV mutant	QPIQIAIVA^{10} LV**FV**IIIAIV^{20} VWSIVIIEYR^{30} K
IVW mutant	QPIQIAIVA^{10} LVVAIIIAIV^{20} **IVSW**VIIEYR^{30} K
IVW-k mutant	QPIQIAIVA^{10} LVVAIIIAIV^{20} **IVSW**VIIEYR^{30} KILRQRKIDR^{40} LIDRLIERAE^{50} DS

The mutations are highlighted in bold and the sequence was adapted from [20]. For model building, a protocol was used which combines a simulated annealing (SA) procedure with short molecular dynamics (MD) simulations based on the program Xplor [21]. This procedure is described in detail elsewhere [22]. The protocol can be briefly summarized as being a two-stage procedure in which in the first stage idealized helices with a rise per residue of 0.15 nm and 3.6 residues per turn were constructed. The tilt angle was set to be 5° for all the helices, either as single entities (see for example [23,24]) or as bundles of five or six helices (see, for example, [23,25]). All atoms of a side chains from a particular residue were superimposed on the Cα-atom. Gradually, the side chain atoms emerge from the position of the Cα-atoms which were restrained in position. During the annealing step (1000 K) weights for bond length, bond angles, planarity and chirality increased. After an initial delay, a repulsive van der Waals term was gradually introduced. Having reached a final scaling factor for the van der Waals term, the structures were cooled to 300 K in steps of 10 K/0.5 ps. To avoid trapping of the side chain atoms in unwanted conformations, the van der Waals radii were reduced to 80% of their full value. This part of the protocol was repeated five times to derive 5 different structures. Each repeat was performed with the different initial velocities needed for a short MD run at 1000 K derived from a Maxwellian random number distribution function. Each of these structures was used in the second stage of the protocol to run 5 short MD simulations at 500 K which differ in their randomly chosen (see above) initial starting velocities. Electrostatic interactions based on the PARAM19 parameter set were introduced at this stage. Harmonic restraints were used to hold the Cα-atoms. These restraints were gradually relaxed while the temperature was reduced from 500 to 300 K. Partial charges on the side chain atoms of the polar side chains were scaled up to a maximum of 0.4 of their full value. At 300 K, a 5 ps MD simulation followed by a 1000-step conjugate gradient energy minimization was performed. The values for the partial charges were also held constant during the 5 ps simulations and minimizations. Distant electrostatic interactions were truncated with a switching function. At the end of the second part of the protocol, 25 structures were generated from which the straightest helix, (in case of the single entities), or the most symmetric model, (for the pseudo five or six fold axes in the bundles), were selected. In general, the bundles were generated by copying a single helix around a central axis holding an inter-helix distance of 0.94 nm.

The extended kinked model, IVW-k was generated from an α-helix as described previously [24] including all the residues, by bending (using SwissPDB viewer software) the helix around residues Glu-28 to Leu-33 so that they adopted the following values at the start of the simulation: $\phi = -59.0°$, $\psi = -25.5°$ for Glu-28; $\phi = -59.2°$, $\psi = -36.1°$ for

Tyr-29; $\phi = -74.5°$, $\psi = -36.5°$ for Arg-30; $\phi = -63.5°$, $\psi = -24.4°$ for Lys-31; $\phi = -25.8°$, $\psi = -54.3°$ for Ile-32; $\phi = -46.7°$, $\psi = -57.3°$ for Leu-33. The generated helix-2 was placed in such a way that Glu-39 was pointing into the phospholipid headgroup region and Arg-48 out of it.

All models were placed in a preequilibrated lipid bilayer of POPC (1-palmitoyl-2-oleoyl-*sn*-glycerol-3-phosphorylcholine) molecules with a cylindrical hole of radius of 0.7 nm and 1.1 nm, for the insertion of the single helix and the bundles, respectively, following the protocol as in [26–28]. Lipid bilayers consisted of 127 and 96 lipid molecules for the simulations of the single TM helix and of the bundles, respectively. The uneven number of lipids in both leaflets for the larger lipid patch has no destabilizing effect on the peptide structure despite the potential for asymmetrical stress to occur in the bilayer [27]. The protein/lipid bilayer system was minimized with the protein coordinates restrained to avoid unfavorable interactions. This was followed by hydration of the system with more than 30 water molecules per lipid and neutralization of the simulation box by the addition of counter ions. After short equilibration runs of about 100 ps with the protein coordinates restrained, the production run was started without any restraints. The total number of atoms in each box was about 20,000 for all the simulations. For IVW-k a bilayer of 261 lipids with 125 for the leaflet, in which helix-2 was embedded, and 136 lipids in the opposing leaflet was used. The 'vacuum' generated by removing the lipids underneath helix-2 was refilled during a 600-ps equilibration phase with the protein restrained in its position within the bilayer. After hydration of the system and addition of counter ions, the simulation box contained a total of ~60,000 atoms. In all models the titratable residues were used in their default ionization state.

For the simulations, GROMACS 3.01 was used, including the simple point charge (SPC) water model. Simulations were run at 300 K in an isothermal-isobaric ensemble (NPT). A constant pressure ($\tau_P = 1.0$ ps independently in all three directions) and temperature ($\tau_T = 0.1$ ps) coupling was applied [29]. Trajectories were calculated in time steps of 2 fs using periodic boundaries and anisotropic pressure coupling. Long range electrostatics were calculated using the particle-mesh Ewald (PME) algorithm with grid dimensions 0.12 nm and interpolation order 4. Lennard–Jones and short-range Coulomb interactions were cut off at 1.0 and 0.9 nm, respectively. The box size typically was within a range of $5.5 \times 5.5 \times 7.5$ nm ($8 \times 10 \times 10$ nm for the simulation with the kinked model). Simulations were run at 300 K. Simulations have been performed on Dell workstations with either dual 1 GHz PIII processors or a 1.4 GHz P4 processor.

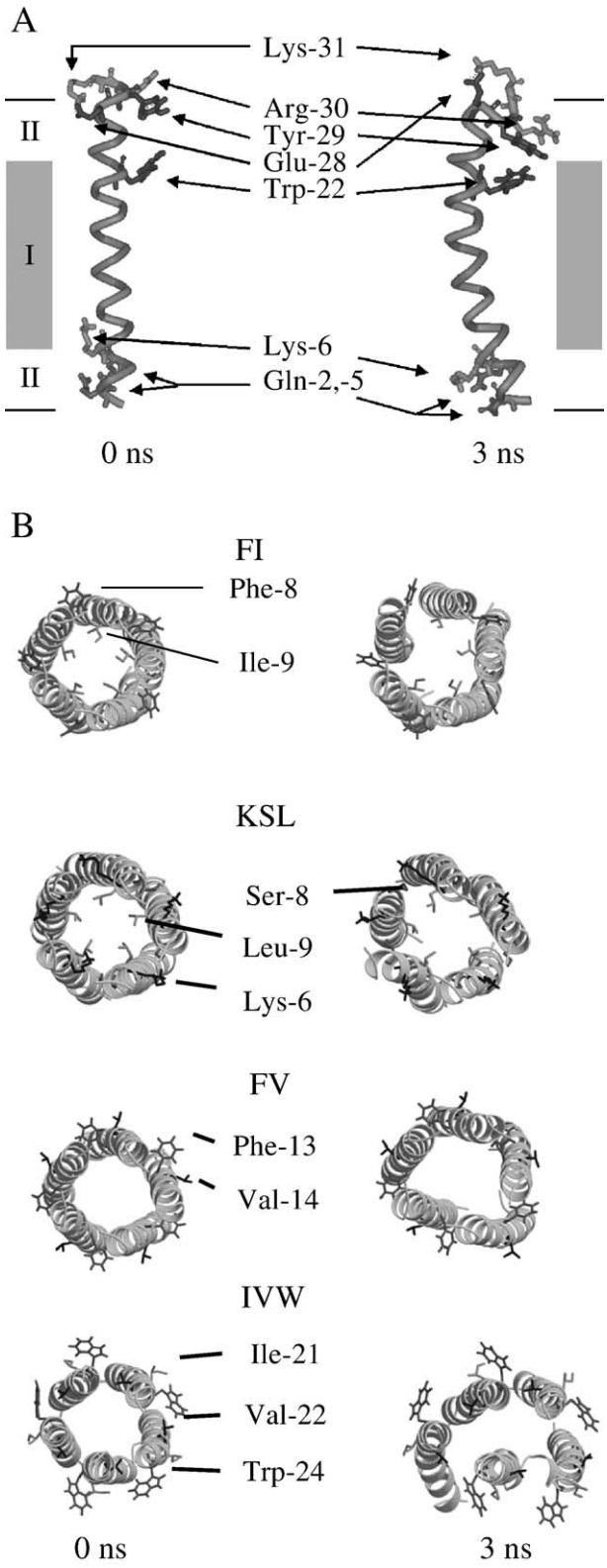

Fig. 1. The structure of the mutant helix KSL-1 at 0 and 3 ns with residues highlighted as indicated (A): Gln-2, -5, Lys-6, -31, Arg-30 (all in light grey); Trp-22, Glu-28 and Tyr-30 (all in dark grey). I and II define the hydrophobic slab and the phospholipid head group region, respectively, of the lipid bilayer. Lipid bilayer and water molecules are omitted. Pentameric models of the mutants FI-5, KSL-5, FV-5 and IVW-5 (B). For FI-5 to FV-5, the view is from the N terminal end, while for IVW-5, the view is from the C terminal end. The mutant residues are highlighted in different grey scales and marked with their names.

3. Results

3.1. Orientation of the mutant residues

A representative single helix of one of the mutants (KSL) is shown in Fig. 1A. During bundle formation, for the FI and KSL bundles, the mutant residues Ile-9 (FI) and Leu-9 (KSL) face the pore (Fig. 1B). Mutated residues, other than those mentioned, do not face the interior of the pore (Fig. 1B). The phenylalanine residues in bundles of FI and FV, as well as the mutant tryptophans in IVW, all point towards the lipid/helix/helix interface. A similar alignment is found for tryptophans in the WT bundle [25,30,31]. All hydrophobic mutated residues point totally towards the hydrophobic slab of the lipid bilayer. The mutant residue Lys-6 in KSL points towards the phospholipid headgroup region, while the mutant residue Ser-8 is located at the helix/helix interface, rather than facing into the pore.

Within the timeframe of a 3-ns production phase of all MD simulations, the displacements of the Cα-atoms of all the consecutive structures from the starting structure do not exceed approximately 0.15–0.25 nm (Fig. 2). Values for all models level off after approximately 500 ps. This level seems to increase with an increasing number of helices involved in the simulations: single helix (Fig. 2A, B) < pentamer (Fig. 2C, D) < hexamer (Fig. 2E, F). Three models deviate from the general behavior in as much as their values do not reach an equilibrated stage (KSL-1, Fig. 2A, dashed black line), or level off at slightly lower (FI-5, Fig. 2C, grey line) or higher values (IVW-5, Fig. 2D, dashed black line) than the other models in their group. In case of KSL-1 this is due to development of a strong kink and an unwinding along residues Ile-27 to Arg-30 at the C terminal end during the simulation (Fig. 1A, right hand side). An unwinding of the C terminal end has also been occasionally observed in simulations of Vpu bundles [25]. One of the helices of IVW-5 is also unwinding at its C terminal end, whereas another helix adopts a strong kink (Fig. 1B). Overall, the bundle seems to 'flatten'. For FI-5 (Fig. 1B), the model seems to represent a structure which has adopted a low energy conformation (see RMSD in Fig. 2C, grey line) because of proper helix–helix packing.

The data for the 'macroscopic' analysis of the models regarding tilt, kink and helix crossing angles, as well as the inter-helical distances, are listed in Table 1. Large tilt angles are found for the single helices. The largest value 19.2° was found for WT-1. All other single helices experience changes with respect to the initial value of about 7–10°. FI-1 seems to remain fairly straight (4.1±2.3°) within the bilayer whereas in all bundles the average tilt angle is considerably larger and comparable to the values found for the mutant bundles. The helices in the pentameric and hexameric bundles adopt angles of around 10°–11°. Large average kink angles are found for the single helices IVW-1 (14.6±2.2°), KSL-1 (32.1±4.3°), FI-1 (16.4±5.1°) and the hexameric bundles FV-6 (17.0±6.0°), KSL-6 (19.5±8.9°).

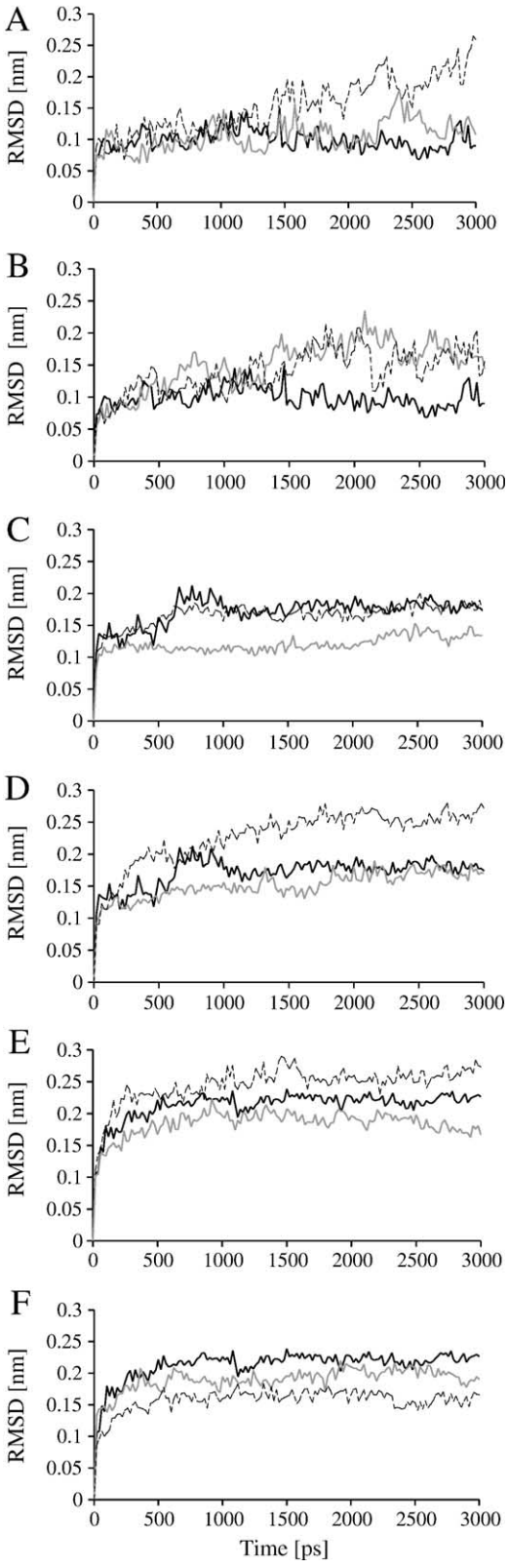

Fig. 2. Root mean square deviation (RMSD) of the Cα atoms of the single helices and the bundles. The graphs contain either WT (black line), FI (grey line) and KSL (dashed black line) for single helix (A), pentamer (C) and hexamer (E), or WT (black line), FV (grey line), and IVW (dashed black line) for single helix (B), pentamer (D), hexamer (F). Data are shown every 20 ps.

Table 1
Averaged tilt, kink, helix crossing angles and averaged inter helical distances

	Tilt [°]	Kink [°]	Helix crossing [°]	Interhelical distance [nm]
WT-1	19.2 ± 2.3	9.4 ± 2.8		
WT-5	8.0 ± 2.7	12.3 ± 7.8	9.3 ± 3.4	1.1 ± 0.0
WT-6	10.7 ± 2.9	16.6 ± 3.8	8.6 ± 6.0	1.0 ± 0.1
FI-1	4.1 ± 2.3	16.4 ± 5.1		
FI-5	13.0 ± 6.9	11.4 ± 4.8	10.4 ± 2.2	1.0 ± 0.0
FI-6	10.2 ± 3.7	13.8 ± 5.2	9.7 ± 3.4	1.0 ± 0.0
KSL-1	10.7 ± 3.1	32.1 ± 4.3		
KSL-5	13.5 ± 6.3	15.5 ± 4.5	12.7 ± 2.9	1.0 ± 0.0
KSL-6	8.6 ± 3.2	19.5 ± 8.9	7.8 ± 3.5	1.1 ± 0.1
FV-1	9.4 ± 1.1	9.9 ± 4.7		
FV-5	12.4 ± 5.2	12.3 ± 5.5	11.2 ± 3.2	1.1 ± 0.1
FV-6	12.2 ± 4.9	17.0 ± 6.0	8.8 ± 3.3	1.04 ± 0.0
IVW-1	14.1 ± 2.0	14.6 ± 2.2		
IVW-5	8.9 ± 3.8	16.6 ± 7.0	9.7 ± 1.7	1.1 ± 0.1
IVW-6	10.1 ± 4.0	13.1 ± 3.9	9.3 ± 3.2	1.0 ± 0.0
IVW-k H1	3.1 ± 1.5	12.3 ± 1.6		

Averages have been taken from the last five frames in steps of 100 ps of the trajectories. 1, 5 and 6 denote the number of helices used in the simulation. H1 stands for the TM helix.

The exceptionally large kink observed for KSL-1 is due to the interaction of the charged residues Lys-6, Glu-28 and Arg-30 residues with the phospholipid headgroup region of the lipid bilayer to achieve a suitable orientation to match the hydrophobic slab of the bilayer. However, when they are assembled to form bundles, the average kink angles of KSL-5 and -6 are within the range found for the other mutant bundles. Hexameric bundles adopt slightly larger average kink angles than the other models. The crossing angles for all bundles are around 10°. The averaged inter-helical distance remains almost the same (~1 nm between the helical axis) for all models.

The analysis of the ϕ- and ψ- angles of the individual mutant amino acids reveal that these values are within the margins typically found for α-helices (data not shown). Thus, the mutations do not have an affect on the local helical conformation of the single strands and the bundles.

The starting structures of all bundles contain a water column. The GROMACS program fits some water molecules into the available space. During the early stage of each simulation, these water molecules disappear and the centre of the pore remains 'empty' for the rest of the simulation. At either end, water pockets are found penetrating about 0.8 nm into the pore. However, several water molecules rapidly cross the 'empty' space (Table 2). There is no obvious directional preference for the water molecules to pass through the pores. In simulations using a cut-off distance for the treatment of the non-bonded long range electrostatic interactions 'empty' pores are not observed. In such simulations, a continuous water column is present for the entire duration of the simulations (data not shown, see also [23,25]).

A typical pore radius profile of the Vpu bundles (WT and mutants) is shown in Fig. 3 for FV-5 (Fig. 3A) and FV-6 (Fig. 3B). For all bundles, including WT, there is a common narrowing of the pore at both the N and C terminal ends, though to a larger extent at the N terminal side. The narrowing is caused by Gln-5 (N-terminus) and Arg-30 (C-terminus). In addition, a narrow region is also found in the middle of the pentameric pores especially around the bulky pore-facing residues Ile-16 and Ile-19. Analysis with the program HOLE [32] reveals that the pore radius, r, would allow only single-file water molecules (1.15 Å$<r<$2.3 Å), especially in the narrow regions within the centre of the pore

Table 2
Traversing water molecules for the WT and mutant bundles

	Traversing water molecules	
	Number	Direction
WT-5	1	↑
WT-6	3	↑↓↓
FI-5	1	↑
FI-6	0	–
KSL-5	0	–
KSL-6	0	–
FV-5	2	↑↓
FV-6	2	↓↓
IVW-5	0	–
IVW-6	2	↑↑

↓ = water moves from C to N terminus, ↑ = water moves from N to C terminus.

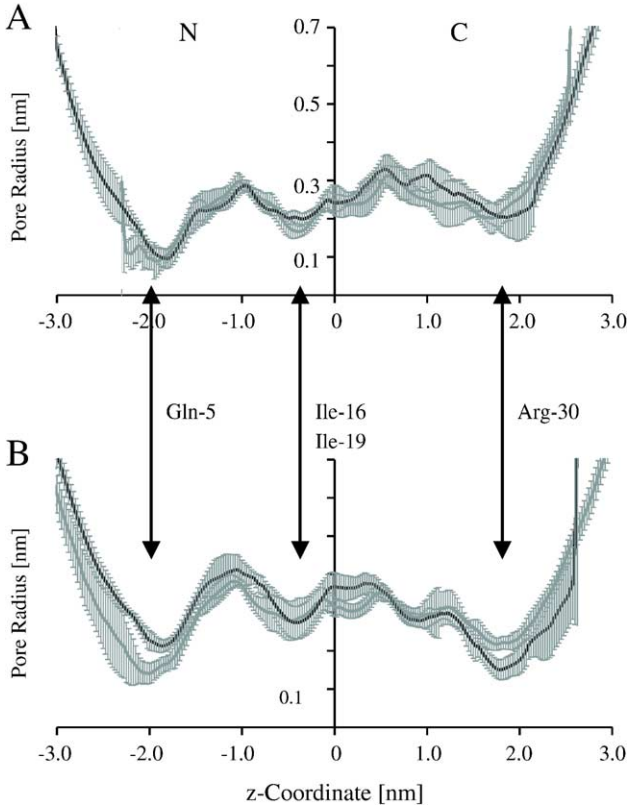

Fig. 3. Averaged pore radius for FV-5 (A) and FV-6 (B) at the beginning (grey trace) of the simulation and at the end (black trace). Arrows from left to right mark the minima in the pore radius caused by residues Gln-5, Ile-16 and -19, as well as Arg-30.

and at the pore mouths. Thus, there is a region in the middle of the pore generating a kind of hydrophobic barrier or 'lock' for ion permeation [33–37]. In the hexameric bundles, this narrow part for the middle of the pore is not observed, allowing for a continuous water column all the way through. The restrictions on the ends still remain but to a lesser extent in the hexameric bundles. In case of the KSL and FI mutants, a narrowing of the pore due to mutant Leu-9 (KSL) and Ile-9 (FI) is not observed (based on calculations with HOLE). Thus, replacing Val-9 with leucine or isoleucine should affect the hydrophobicity within the pore rather than the overall pore geometry.

3.2. The kinked mutant IVW-k

The kinked model IVW-k is constructed in such a way that the helix is bent around residues Glu-28 to Leu-33 keeping them as far as possible in a helical conformation [24]. The part of the long helix lying on top of the bilayer after the bend is called helix-2. The bend was performed so that helix-2 would not interfere with bundle formation and that the hydrophilic residue Ser-23 would face into the pore. The uneven number of lipids taken out from the two leaflets of the bilayer causes a perturbation in the system [24]. The hydrophobic tails of the lipid molecules crawl underneath helix-2, leading to a reduced lateral pressure in the hydrophobic slab of this leaflet. Since any protein–lipid interaction would induce this membrane perturbation of moving more lipids away in one leaflet than in the other, this model is one which most closely resembles the natural environment: helix-2 has all its hydrophobic residues facing the bilayer and the interaction with the hydrophobic tails of the lipids rather than with the polar headgroups would be energetically favorable while the hydrophilic residues of helix-2 point towards the aqueous phase.

The RMSDs of the Cα atoms of the simulation on IVW-k level off after approximately 500 ps at a higher level (around 0.4 nm, Fig. 4A) than found for the bundle simulations (Fig. 2C–F). This difference is due to a heavy unwinding beyond the region of the bend including residues in helix-2 up to Lys-37/Ile-38. Unwinding is initiated by the mutant Trp-24 which is located just underneath the bend of helix-2 at the start of the simulation (Fig. 4B). At this position, it clashes with residues in helix-2 such as Glu-28 and Lys-31. In the

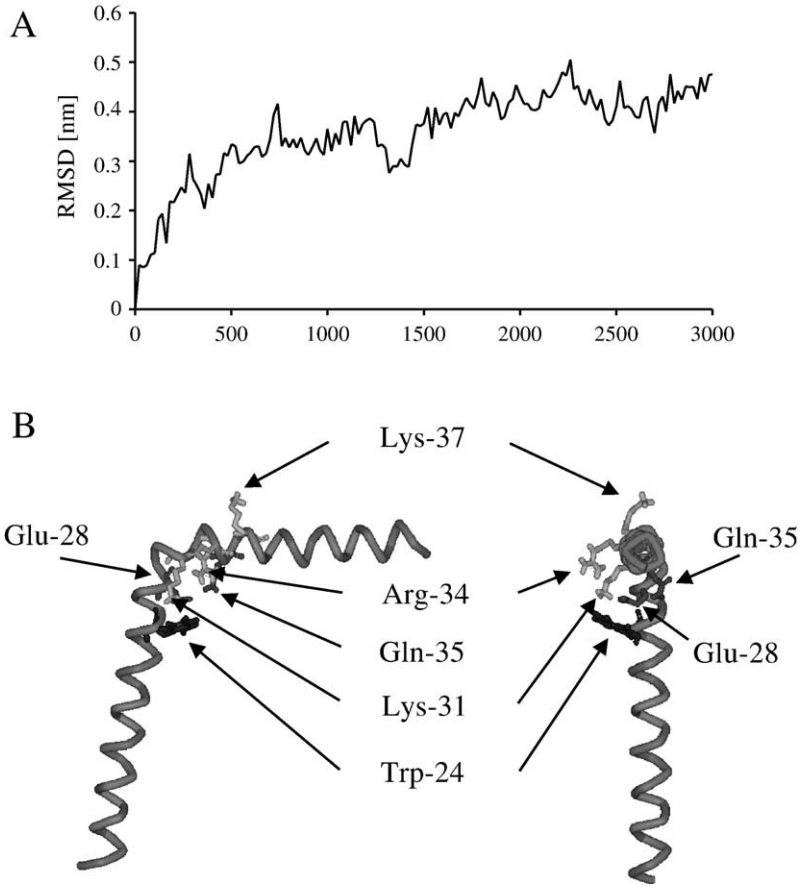

Fig. 4. Root mean square deviation (RMSD) of the Cα-atoms of the kinked mutant IVW-k (A). Data are shown every 20 ps. Starting structure of IVW-k is shown in a side view (B, left hand side) and from the C terminal end along the helix axis of helix-2 (B, right hand side). Lipids and water molecules are omitted. Trp-24, Glu-28, Gln-35 are shown in dark grey. Lys-31, Arg-34 and Lys-37 are shown in light grey. IVW-k is generated from a single helix which is bent (using SwissPDB viewer software) around residues Glu-28 to Leu-33. Helix-2 is consequently lies on top of the lipid bilayer. Ser-23, within the TM helix, is pointing away from helix-2.

starting configuration, Glu-28, Lys-31, Arg-34, Gln-35 form a complex salt bridge (Fig. 5, 0 ns), while Lys-37 faces the aqueous phase. Throughout the simulation (Fig. 5, 1 and 2 ns), the unwinding of the N terminal part of helix-2 is accompanied by a replacement of Arg-34 by Lys-37 within the formation of the complex salt bridge (Fig. 5, at 3 ns). In the simulation, Tyr-29 and Arg-30 approach each other forming hydrogen bonds (data not shown). The disruption of parts of the helical structure of helix-2 can also be visualized by the percentage of the simulation time a residue remains in a helical conformation (Fig. 6). Residues Glu-28 to Ile-38, which are part of helix-2 in the WT model [24], spend a very low percentage of the simulation time in a helical conformation in the mutant model.

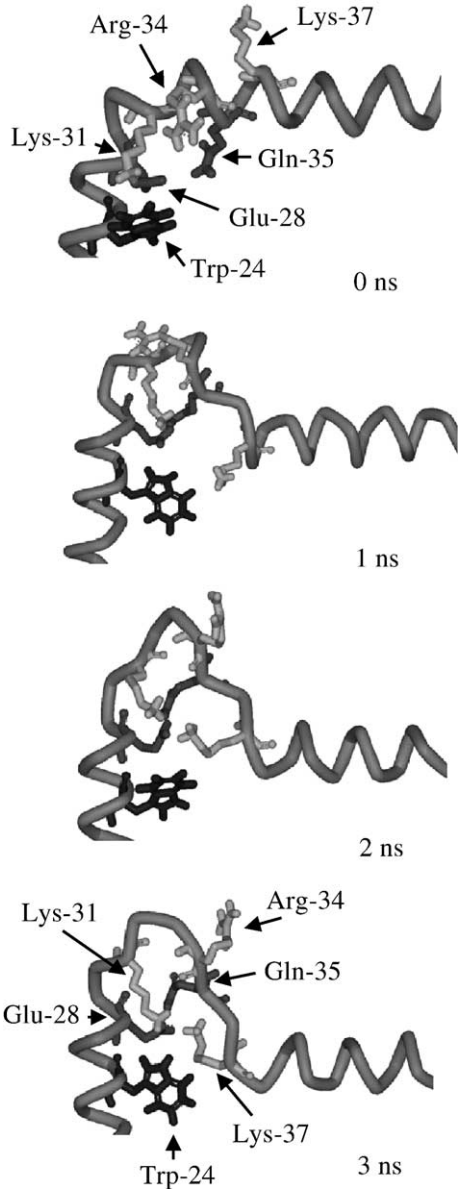

Fig. 5. Expanded view of the bend region of IVW-k shown in Fig. 4B at 0, 1, 2 and 3 ns. Trp-24, Glu-28, Gln-35 are shown in dark grey. Lys-31, Arg-34 and Lys-37 are shown in light grey. The evolution of structural changes is shown in a side view. The complex salt bridge formed by Glu-28, Lys-31, Arg-34 and Gln-35 at the beginning of the simulation (0 ns) is replaced by a complex salt bridge formed by the same residues except for a replacement of Arg-34 by Lys-37.

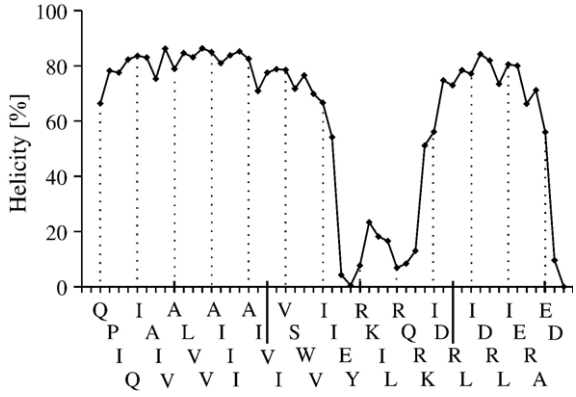

Fig. 6. Relative helicity (in %) of the residues in IVW-k based on their C α coordinates. The entire range of the simulation is contributing for the calculations. Residues Glu-28 to Arg-36 are less then 30% of their time in a helical conformation. Every tenth residue is indicated by a bar, dotted lines indicate the residues placed directly at the ordinate.

The overall effect of the structure of the second helix in the extended model on the tilt angle of the TM helix is moderate (Table 1). Starting with 7.2±3.9°, the tilt angle passes a maximum angle of approximately 12–14° at around 500 ps and remains tilted at around 3.1±1.5° until the end of the simulation. The angle between TM helix and helix-2 adopts a value of around 100° towards the end of the simulation, which is in agreement with the results of a simulation with a kinked Vpu (Vpu_{1-52}) model reported in an earlier study [24]. The kink angle of the TM helix remains almost constant with starting and final values of 10.3±1.6° and 12.3±1.6°, respectively. Because of the large scale unwinding of helix-2, kink and tilt angles cannot be measured.

4. Discussion

4.1. The TM domains

The bundles are built in such a way that they match our current knowledge of water-filled ion-conducting membrane proteins. Hydrophilic residues, such as serines, within a hydrophobic TM helix face the lumen of the pore. Any aromatic residues, especially tryptophans, should help to anchor the protein within the lipid bilayer and would be located at the putative ends of a TM helix and facing a helix–helix–lipid interface. Investigation of the mutants demonstrates the integrity of the single helix, the pentameric and hexameric bundles embedded in a lipid bilayer. In one example (IVW-5), the bundle adopts a flattened structure. Such non-ideal bundles seem to result from unfavorable interactions which occur during the energy minimization and short equilibration runs prior to the production phase. Similar flattened bundles have also been observed recently in simulation of hexameric Vpu bundles [31].

WT and mutants adopt tilt angles perfectly matching experimental findings of the WT peptide [38]. Any biological effect of the mutations mentioned by Tiganos et al. [20] may not be caused by large structural disturbance.

Any mutation within the TM helix can potentially abrogate channel activity. The data presented here suggest that most of the mutations do not affect the environment of the interior of the pore, and consequently it is assumed that channel activity is not affected. The only exceptions might be the FI and KSL mutants, both of which have the mutant residue pointing into the lumen of the pore.

The experimentally observed effect of the mutations in [20] may also be due to interaction with other membrane proteins, e.g. ion channels (such as TASK-1 [39]), at the site of the plasma membrane. Thus, Vpu might also be indirectly involved in altering electrochemical gradients [39]. From the simulations presented in this study, it seems likely that the mutations should not interfere with ion channel activity. Experiments with the mutants would need to be performed to validate this claim.

4.2. Water within the pore

A series of computational studies of water molecules in narrow geometries have revealed that the presence of water is dependent on a series of parameters such as pore length, diameter and polarity of the lining residues [37,40–43]. In the case of Vpu, diameters of less than 0.6 nm are adopted which account for the absence of single-file water molecules observed in gramicidin A [44–47]. The pore radius does not increase even in longer simulations of more than 50 ns (Lemaitre, Fischer, unpublished results).

4.3. PME versus cut off

In earlier simulations, any long range electrostatic interactions after the cut off distance were neglected [25]. Vpu bundles with water-filled pores were observed. Calculations with electrostatic force truncation have shown an increased structuring of water [48] and an decrease of translational and rotational motion [49]. These effects may also be present at the single water level as found in the narrow pores leading to the artificially prolonged presence of water molecules in the pore at least for the times spans covered in the simulations reported earlier [25]. The use of PME in the present study ejects water from the beginning of the simulation, even though the pore is wide enough to allow solvent molecules to be situated within it. There is only a small pocket of water molecules left at the C terminal mouth of the bundles. PME is now widely used for simulations on biomolecules [50–52] since simulations result in stable protein structures [53]. The method can also be used independent of the size of the system if it is slightly modified [54]. The method is not free of artefacts such as, e.g., the biasing of the rotation of biomolecules due to artificial periodicity [55]. However, it has been shown that high relative permittivity of the solvent permits these artefacts to be ignored when simulating biomolecules [56]. Simulations on K^+-channel models using PME rather than cut-off for the long range electrostatic interactions appear to show little difference in the dynamics of the water molecules [57]. Thus, the disappearing of the water molecules may represent a more accurate picture of the channel behavior.

4.4. Hydrophobic gate

The TM helix of Vpu contains a long hydrophobic sequence which causes a constriction around Ile-16 and Ile-19 in a homo-oligomeric bundle. These residues probably establish a hydrophobic barrier for ions and water molecules and might represent a ‘hydrophobic gate’ [33,58]. Hydrophobic barriers or locks are established features in the nAChR [59,60], the mechanosensitive channel MscL [35] and the potassium channel KcsA [58,61–63].

4.5. The extended kinked model

The IVW mutant is the only mutant which not only abrogates particle release but is also unable to induce CD4 degradation [20]. In the light of the present data, it is suggested that the mutant cannot adopt a functional conformation especially for the cytoplasmic domain. The chosen conformation is created by the partial unwinding of helix-2, which probably leads to further conformational disruption towards the C terminal end. It is also possible, however, that initially the mutant would not adopt such a conformation and instead would remain in a non-functional conformation. This strengthens the idea of a well-defined conformation between the TM helix and helix-2 as suggested in [24], which is essential for Vpu to fulfill its role of inducing CD4 degradation.

4.6. Short versus long simulations

In this study, the emphasis has been on screening a large number of mutants in a short time. Therefore, relatively short simulation time frames have been chosen. In comparison with data from longer simulations of selected mutants (Lemaitre and Fischer unpublished results), no major differences regarding the overall structural analysis of the data have been found.

5. Conclusions

Computer simulations will play a major part in future investigations on the understanding of protein mechanisms of function (biochemical proteomics), especially when structure based information is necessary for the development of novel drugs. In this study, we have tried to correlate experimental findings on the function of Vpu mutants with

structural alterations which occur in the protein. Within the boundaries of our current MD simulations, the helicity of all mutants and their integrity in a bundle do not show major deviation from the WT structure. Correlating this to the functioning, the effect of the mutant as reported in Tiganos et al. [20] may be looked for at the site of the TASK-1–Vpu interaction. In case of one of the mutants, in which the only tryptophan in the TM region is shifted up in the sequence, there is an impact on the structure of the second helix in the protein. This result can be related with the experimental findings of the inability of this mutant to degrade CD4.

Acknowledgements

This work is supported by the E.P. Abraham Research Fund to AW and WBF, a BBSRC Fellowship to AW, and support from MRC. Thanks to P. Judge (Oxford) for valuable discussions.

References

[1] S. Huo, I. Massova, P.A. Kollman, Computational alanine scanning of the 1:1 human growth hormone–receptor complex, J. Comput. Chem. 23 (2002) 15–27.
[2] S. Kamath, T.C. Wong, Membrane structure of the human immunodeficiencey virus gp41 fusion domain by molecular dynamics simulations, Biophys. J. 83 (2002) 135–143.
[3] T.C. Wong, Membrane structure of the human immunodeficiency virus gp41 fusion peptide by molecular dynamics simulation: II. The glycine mutant, Biochim. Biophys. Acta 1609 (2003) 45–54.
[4] K. Strebel, T. Klimkait, M.A. Martin, Novel gene of HIV-1, *vpu*, and its 16-kilodalton product, Science 241 (1988) 1221–1223.
[5] E.A. Cohen, E.F. Terwilliger, J.G. Sodroski, W.A. Haseltine, Identification of a protein encoded by the *vpu* gene of HIV-1, Nature 334 (1988) 532–534.
[6] F. Maldarelli, M.Y. Chen, R.L. Willey, K. Strebel, Human-immunodeficiency- virus type-1 Vpu protein is an oligomeric type-I integral membrane protein, J. Virol. 67 (1993) 5056–5061.
[7] W.B. Fischer, M.S.P. Sansom, Viral ion channels: structure and function, Biochim. Biophys. Acta 1561 (2002) 27–45.
[8] K. Strebel, T. Klimkait, F. Maldarelli, M.A. Martin, Molecular and biochemical analysis of human deficiency virus type 1 *vpu* protein, J. Virol. 63 (1989) 3784–3791.
[9] R.L. Willey, F. Maldarelli, M.A. Martin, K. Strebel, Human immunodeficiency virus type 1 Vpu protein induces rapid degradation of CD4, J. Virol. 66 (1992) 7193–7200.
[10] U. Schubert, A.V. Ferrer-Montiel, M. Oblatt-Montal, P. Henklein, K. Strebel, M. Montal, Identification of an ion channel activity of the Vpu transmembrane domain and its involvement in the regulation of virus release from HIV-1-infected cells, FEBS Lett. 398 (1996) 12–18.
[11] S. Bour, U. Schubert, K. Strebel, The human immunodeficiency virus type 1 Vpu protein specifically binds to the cytoplasmic domain of CD4: implications for the mechanism of degradation, J. Virol. 69 (1995) 1510–1520.
[12] U. Schubert, S. Bour, A.V. Ferrer-Montiel, M. Montal, F. Maldarelli, K. Strebel, The two biological activities of human immunodeficiency virus type 1 Vpu protein involve two separable structural domains, J. Virol. 70 (1996) 809–819.
[13] M. Paul, S. Mazumder, N. Raja, M.A. Jabbar, Mutational analysis of the human immunodeficiency virus type 1 Vpu transmembrane domain that promotes the enhanced release of virus-like particles from the plasma membrane of mammalian cells, J. Virol. 72 (1998) 1270–1279.
[14] V. Wray, T. Federau, P. Henklein, S. Klabunde, O. Kunert, D. Schomburg, U. Schubert, Solution structure of the hydrophilic region of HIV-1 encoded virus protein U (Vpu) by CD and ^{1}H NMR-spectroscopy, Int. J. Pept. Protein Res. 45 (1995) 35–43.
[15] T. Federau, U. Schubert, J. Floßdorf, P. Henklein, D. Schomburg, V. Wray, Solution structure of the cytoplasmic domain of the human immunodeficiency virus type 1 encoded virus protein U (Vpu), Int. J. Pept. Protein Res. 47 (1996) 297–310.
[16] D. Willbold, S. Hoffmann, P. Rösch, Secondary structure and tertiary fold of the human immunodeficiency virus protein U (Vpu) cytoplasmatic domain in solution, Eur. J. Biochem. 245 (1997) 581–588.
[17] C. Ma, F.M. Marassi, D.H. Jones, S.K. Straus, S. Bour, K. Strebel, U. Schubert, M. Oblatt-Montal, M. Montal, S.J. Opella, Expression, purification, and activities of full-length and truncated versions of the integral membrane protein Vpu from HIV-1, Protein Sci. 11 (2002) 546–557.
[18] V. Wray, R. Kinder, T. Federau, P. Henklein, B. Bechinger, U. Schubert, Solution structure and orientation of the transmembrane anchor domain of the HIV-1-encoded virus protein U by high resolution and solid-state NMR spectroscopy, Biochemistry 38 (1999) 5272–5282.
[19] A. Kukol, I.T. Arkin, Vpu transmembrane peptide structure obtained by site-specific Fourier transform infrared dichroism and global molecular dynamics searching, Biophys. J. 77 (1999) 1594–1601.
[20] E. Tiganos, J. Friborg, B. Allain, N.G. Daniel, X.-J. Yao, E.A. Cohen, Structural and functional analysis of the membrane-spanning domain of the Human Immunodeficiency Virus Type 1 Vpu protein, Virology 251 (1998) 96–107.
[21] A.T. Brünger, X-PLOR Version 3.1. A System for X-ray Crystallography and NMR, Yale Univ. Press, New Haven, CT, 1992.
[22] I.D. Kerr, R. Sankararamakrishnan, O.S. Smart, M.S.P. Sansom, Parallel helix bundles and ion channels: molecular modelling via simulated annealing and restrained molecular dynamics, Biophys. J. 67 (1994) 1501–1515.
[23] W.B. Fischer, M. Pitkeathly, B.A. Wallace, L.R. Forrest, G.R. Smith, M.S.P. Sansom, Transmembrane peptide NB of influenza B: a simulation, structure, and conductance study, Biochemistry 39 (2000) 12708–12716.
[24] I. Sramala, V. Lemaitre, J.D. Faraldo-Gomez, S. Vincent, A. Watts, W.B. Fischer, Molecular dynamics simulations on the first two helices of Vpu from HIV-1, Biophys. J. 84 (2003) 3276–3284.
[25] F.S. Cordes, A. Tustian, M.S.P. Sansom, A. Watts, W.B. Fischer, Bundles consisting of extended transmembrane segments of Vpu from HIV-1: computer simulations and conductance measurements, Biochemistry 41 (2002) 7359–7365.
[26] D.P. Tieleman, M.S.P. Sansom, H.J.C. Berendsen, Alamethicin helices in a bilayer and in solution: molecular dynamics simulations, Biophys. J. 76 (1999) 40–49.
[27] L.R. Forrest, D.P. Tieleman, M.S.P. Sansom, Defining the transmembrane helix of M2 protein from influenza A by molecular dynamics simulations in a lipid bilayer, Biophys. J. 76 (1999) 1886–1896.
[28] L.R. Forrest, A. Kukol, I.T. Arkin, D.P. Tieleman, M.S. Sansom, Exploring models of the influenza A M2 channel: MD simulations in a phospholipid bilayer, Biophys. J. 78 (2000) 55–69.
[29] H.J.C. Berendsen, J.P.M. Postma, W.F. van Gunsteren, A. Di Nola, J.R. Haak, Molecular dynamics with coupling to an external bath, J. Chem. Phys. 81 (1984) 3684–3690.
[30] A.L. Grice, I.D. Kerr, M.S.P. Sansom, Ion channels formed by HIV-1 Vpu: a modelling and simulation study, FEBS Lett. 405 (1997) 299–304.
[31] C.F. Lopez, M. Montal, J.K. Blasie, M.L. Klein, P.B. Moore,

Molecular dynamics investigation of membrane-bound bundles of the channel-forming transmembrane domain of viral protein U from the Human Immunodeficiency Virus HIV-1, Biophys. J. 83 (2002) 1259–1267.
[32] O.S. Smart, J.G. Neduvelil, X. Wang, B.A. Wallace, M.S.P. Sansom, Hole: a program for the analysis of the pore dimensions of ion channel structural models, J. Mol. Graph. 14 (1996) 354–360.
[33] O. Beckstein, P.C. Biggin, M.S.P. Sansom, A hydrophobic gating mechanism for nanopores, J. Phys. Chem. B 105 (2001) 12902–12905.
[34] N. Unwin, Structure and action of the nicotinic acetylcholine receptor explored by electron microscopy, FEBS Lett. 555 (2003) 91–95.
[35] G. Chang, R.H. Spencer, A.T. Lee, M.T. Barclay, D.C. Rees, Structure of the MscL homolog from *Mycobacterium tuberculosis*: a gated mechanosensitive ion channel, Science 282 (1998) 2220–2226.
[36] P.C. Moe, G. Levin, P. Blount, Correlating a protein structure with function of a bacterial mechanosensitive channel, J. Biol. Chem. 275 (2000) 31121–31127.
[37] A. Anishkin, S. Sukharev, Water dynamics and dewetting transitions in the small mechanosensitive channel MscS, Biophys. J. 86 (2004) 2883–2895.
[38] S.H. Park, A.A. Mrse, A.A. Nevzorov, M.F. Mesleh, M. Oblatt-Montal, M. Montal, S.J. Opella, Three-dimensional structure of the channel-forming trans-membrane domain of virus protein "u" (Vpu) from HIV-1, J. Mol. Biol. 333 (2003) 409–424.
[39] K. Hsu, J. Seharaseyon, P. Dong, S. Bour, E. Marbán, Mutual functional destruction of HIV-1 Vpu and host TASK-1 channel, Mol. Cell 14 (2004) 259–267.
[40] E. Spohr, A. Trokhymchuk, D. Henderson, Adsorption of water molecules in slit pores, J. Electroanal. Chem. 450 (1998) 281–287.
[41] G. Hummer, J.C. Rasaiah, J.P. Noworyta, Water conducting through the hydrophobic channel of a carbon nanotube, Nature 414 (2001) 188–190.
[42] R. Allen, J.-P. Hansen, S. Melchionna, Molecular dynamics investigation of water permeation through nanopores, J. Chem. Phys. 119 (2003) 3905–3919.
[43] O. Beckstein, M.S.P. Sansom, The influence of geometry, surface character, and flexibility on the permeation of ions and water through biological pores, Phys. Biol. 1 (2004) 42–52.
[44] B. Roux, M. Karplus, Ion transport in a model gramicidin channel: structure and thermodynamics, Biophys. J. 59 (1991) 961–981.
[45] G.A. Woolley, B.A. Wallace, Model ion channels: gramicidin and alamethicin, J. Membr. Biol. 129 (1992) 109–136.
[46] S.-W. Chiu, S. Subramaniam, E. Jakobsson, Simulation study of a gramicidin/lipid bilayer system in excess water and lipid: I. Structure of the molecular complex, Biophys. J. 76 (1999) 1929–1938.
[47] B.L. de Groot, D.P. Tieleman, P. Pohl, H. Grubmüller, Water permeation through gramicidin A: desformylation and the double helix: a molecular dynamics study, Biophys. J. 82 (2002) 2934–2942.
[48] S.E. Feller, R.W. Pastor, A. Rojnuckarin, S. Bogusz, B.R. Brooks, Effect of electrostatic force truncation on interfacial and transport properties of water, J. Phys. Chem. 100 (1996) 17011–17020.
[49] W.F. van Gunsteren, H.J.C. Berendsen, J.A.C. Rullmann, Inclusion of reaction fields in molecular dynamics: application to liquid water, Faraday Discuss. Chem. Soc. 66 (1978) 58–70.
[50] F. Figueirido, G.S. Del Buono, R.M. Levy, On finite-size effects in computer simulations using the Ewald potential, J. Chem. Phys. 103 (1995) 6133–6142.
[51] B.A. Luty, W.F. van Gunsteren, Calculating electrostatic interactions using the particle–particle particle–mesh method with nonperiodic long-range interactions, J. Phys. Chem. 100 (1996) 2581–2587.
[52] T. Hansson, C. Oostenbrink, W.F. van Gunsteren, Molecular dynamics simulations, Curr. Opin. Struct. Biol. 12 (2002) 190–196.
[53] H. Schreiber, O. Steinhauser, Cutoff size does strongly influence molecular dynamics results on solvated polypeptides, Biochemistry 31 (1992) 5856–5860.
[54] U. Essmann, L. Perera, M.L. Berkowitz, T. Darden, H. Lee, L.G. Pedersen, A smooth particle mesh Ewald method, J. Chem. Phys. 103 (1995) 8577–8593.
[55] P.E. Smith, B.M. Pettitt, Ewald artifacts in liquid state molecular dynamics simulations, J. Chem. Phys. 105 (1996) 4289–4293.
[56] P.E. Smith, H.D. Blatt, B.M. Pettitt, On the presence of rotational Ewald artifacts in the equilibrium and dynamical properties of a zwitterionic tetrapeptide in aqueous solution, J. Phys. Chem. B 101 (1997) 3886–3890.
[57] C.E. Capener, M.S.P. Sansom, Molecular dynamics simulations of a K channel model: sensitivity to changes in ions, waters, and membrane environment, J. Phys. Chem. B 106 (2002) 4543–4551.
[58] B. Roux, S. Berneche, W. Im, Ion channels, permeation, and electrostatics: insight into the function of KcsA, Biochemistry 39 (2000) 13295–13306.
[59] N. Unwin, Nicotinic acetylcholine receptor at 9 Å resolution, J. Mol. Biol. 229 (1993) 1101–1124.
[60] N. Unwin, Acetylcholine receptor channel imaged in the open state, Nature 373 (1995) 37–43.
[61] D.A. Doyle, J.M. Cabral, R.A. Pfuetzner, A. Kuo, J.M. Gulbis, S.L. Cohen, B.T. Chait, R. MacKinnon, The structure of the potassium channel: molecular basis of K^+ conduction and selectivity, Science 280 (1998) 69–77.
[62] T.W. Allen, A. Bliznyuk, A.P. Rendell, S. Kuyucak, S.-H. Chung, The potassium channel: structure, selectivity and diffusion, J. Chem. Phys. 112 (2000) 8191–8204.
[63] P.C. Biggin, G.R. Smith, I.H. Shrivastava, S. Choe, M.S.P. Sansom, Potassium and sodium ions in a potassium channel studied by molecular dynamics simulations, Biochim. Biophys. Acta 1510 (2001) 1–9.